

Self-supervised Learning with Geometric Constraints in Monocular Video

Connecting Flow, Depth, and Camera

Yuhua Chen¹ Cordelia Schmid² Cristian Sminchisescu²

¹ETH Zurich ²Google Research

yuhua.chen@vision.ee.ethz.ch, {cordelias, sminchisescu}@google.com

Abstract

We present **GLNet**, a self-supervised framework for learning depth, optical flow, camera pose and intrinsic parameters from monocular video – addressing the difficulty of acquiring realistic ground-truth for such tasks. We propose three contributions: 1) we design new loss functions that capture multiple geometric constraints (e.g. epipolar geometry) as well as adaptive photometric costs that support multiple moving objects, rigid and non-rigid, 2) we extend the model such that it predicts camera intrinsics, making it applicable to uncalibrated video, and 3) we propose several online finetuning strategies that rely on the symmetry of our self-supervised loss in both training and testing, in particular optimizing model parameters and/or the output of different tasks, leveraging their mutual interactions. The idea of jointly optimizing the system output, under all geometric and photometric constraints can be viewed as a dense generalization of classical bundle adjustment. We demonstrate the effectiveness of our method on KITTI and Cityscapes, where we outperform previous self-supervised approaches on multiple tasks. We also show good generalization for transfer learning.

1. Introduction

One of the fundamental computer vision problems is estimating the three-dimensional geometry of dynamic scenes captured by a moving camera. This encompasses many visual tasks such as the estimation of depth, optical flow or visual odometry. Robust solutions would support a wide range of applications in autonomous driving, robotics, virtual and augmented reality, or scene interaction.

The 3D visual reconstruction problem has been studied extensively. At one end, there are structure from motion systems [13] that leverage sparse, hand-crafted geometric features (e.g. SIFT [26] or SURF [1]), exact linear mathematical relations [13] (e.g. the epipolar constraint and the fundamental matrix for the two view geometry), as well as

the non-linear refinement of the structure and motion outputs under geometric re-projection losses based on bundle adjustment [37]. Impressive real-time processing pipelines of this type are now available, but they still offer sparse reconstructions, are affected by partial occlusion, and face difficulties in cases when the geometry of the scene or the motion is degenerate.

At the other end, recent years have witnessed the development of deep learning techniques where structure and motion estimation is formulated in a supervised setting, as a pure prediction problem with little reference to exact geometric relations. This produces dense 3D estimates but comes with the inherent limitation of possible geometric inconsistency, the dependence on large training sets, and the difficulty of collecting good quality real-world ground-truth using special equipment like laser or stereo rigs with sensitive calibration [10]. Another option is to use synthetic data [28], however bridging the realism gap can be challenging.

More recently, several authors [12, 48] focused on designing self-supervised systems with training signals resulting from photometric consistency losses between pairs of images. These systems are effective and implicitly embed basic 3D geometry – as points in the first view are back-projected in 3D, displaced by the camera motion and re-projected in the second view –, but still lack the fundamental geometric constraints that link the rigid and apparent motion in multiple views.

In this work we introduce a self-supervised geometric learning framework, **GLNet**, which aims to integrate the advantages of modern deep-learning based self-supervised systems – (a) training without labeled data, (b) offering dense reconstructions where prior knowledge can be automatically incorporated, and (c) leveraging multiple interconnected tasks –, with the ones of classical structure from motion – (i) explicitly representing exact mathematical relations (e.g. the epipolar constraint) that always hold, (ii) being able to jointly refine all outputs, including depth, pose and camera intrinsics, under adaptive photometric and geo-

metric constraints, as in bundle adjustment, and (iii) breaking asymmetries between training and testing.

The proposed framework is extensively evaluated on KITTI and Cityscapes, where we achieve performance gains over the state-of-the-art. Moreover, our framework shows good performance in a transfer learning setting, and is able to robustly learn from uncalibrated video.

2. Related Work

Understanding the geometry and dynamics of 3D scenes usually involves estimating multiple properties including depth, camera motion or optical flow. *Structure from motion* (SfM) [8, 13, 31, 35, 37, 42] or scene flow estimation [30, 38] are well-established methodologies with a solid record of fundamental and practical progress. Classical approaches are based on low-level feature matching followed by geometric verification using algebraic relations, *e.g.* the epipolar constraint, in conjunction with RANSAC [3], and bundle adjustment [37]. Models for structure and motion estimation based on such pipelines have produced impressive results [35], but their reconstructions are often sparse and prone to error in textureless or occluded areas.

To address the bottleneck of accurate feature matching, recent work has focused on deep-learning-based approaches for geometric reasoning. Several methods train networks based on ground-truth labels and have been successfully applied to many tasks, including monocular depth estimation [6, 7, 24, 25], optical flow [5, 15, 32, 36], geometric matching [33], disparity from stereo images [21], or camera pose estimation [18, 19, 20]. Because often geometric reasoning tasks are intrinsically coupled, several methods aim to leverage their inter-dependencies by joint supervision [34, 46]. Ilg *et al.* [16] jointly estimate disparity, flow and boundaries. Depth estimation is also shown to benefit from combining with surface normals [25].

To train using ground-truth labels, different authors rely either on synthetic dataset creation [28] or on specialized equipment (*e.g.* LIDAR) for data collection [10, 11], which is expensive in practice. To reduce the amount of ground-truth labels required for training, unsupervised approaches recently emerged. The core idea is to generate a differentiable warping between two images and use an underlying photometric loss as proxy to train a self-supervised model. This has been applied to stereo images [9, 12, 47] and optical flow [17, 29, 43].

In this work, we focus on learning from monocular video. Many recent methods go along similar lines. Zhou *et al.* [48] couple the learning of monocular depth and ego-motion. Vijayanarasimhan *et al.* [39] learn object masks and rigid motion parameters of several objects. Subsequent methods further improved performance using various techniques, Mahjourian *et al.* [27] compute a 3D loss using ICP,

and Klodt *et al.* [23] use a supervision term that relies on the SfM output to regularize and unsupervised learning process. The learning can be facilitated by integrating other cues such as optical flow [45, 49], edges [44] or modeling multiple rigid motions [2].

3. Methodology

Overview Our Geometric Learning Network (GLNet), for which an overview is presented in fig. 1, solves the inter-related tasks of monocular depth prediction, optical flow, camera pose and intrinsics estimation, by relying on predictors for depth \mathbf{D}_θ , camera \mathbf{C}_α and flow \mathbf{F}_δ within a coupled training loss. \mathbf{D}_θ is parameterized by θ , and estimates the depth map \mathbf{D} from a single image. \mathbf{C}_α predicts the camera pose (\mathbf{R}, \mathbf{t}) between two adjacent frames, and also the intrinsic parameters \mathbf{K} whenever unknown. \mathbf{F}_δ operates on two image frames and estimates the optical flow. The joint output space of the tasks is denoted as $\Lambda = \{\mathbf{D}, \mathbf{R}, \mathbf{t}, \mathbf{K}, \mathbf{F}\}$, where the superset of parameters is $\Theta = \{\theta, \delta, \alpha\}$. The predictors are implemented as three neural networks with trainable parameters, referred to as *DepthNet*, *CameraNet* and *FlowNet* respectively.

We formulate an optimization objective which consists of two parts: an adaptive photometric consistency loss that captures the appearance similarity of the static and dynamic structures, and a geometric loss consisting of several components that couple the rigid and apparent motion. In training, the optimization objective is used as a proxy supervision signal to learn the predictor parameters Θ . During inference, we can further refine the predictions based on the same criterion used in training, and we are able to focus on either refining the model parameters or the outputs, not unlike in geometric bundle adjustment. This is enabled by our self-supervised objective and our explicit representation of classical geometric constraints.

3.1. Geometric and Appearance Fundamentals

Consider a source image I^s and a target image I^t , collected by a potentially moving camera with intrinsics \mathbf{K}_α and ego-motion \mathbf{M}_α . The 3D rigid transformation can be represented in homogeneous coordinates, in terms of a rotation matrix and a translation vector as

$$\mathbf{M}_\alpha = \begin{bmatrix} \mathbf{R}_\alpha & \mathbf{t}_\alpha \\ 0 & 1 \end{bmatrix} \quad (1)$$

For camera intrinsics, we fix the optical center at the image center, ignore camera skew and radial distortion, parameterize as f^x and f^y the focal length along the two optical axes, and have images with resolution $h \times w$. The intrinsics

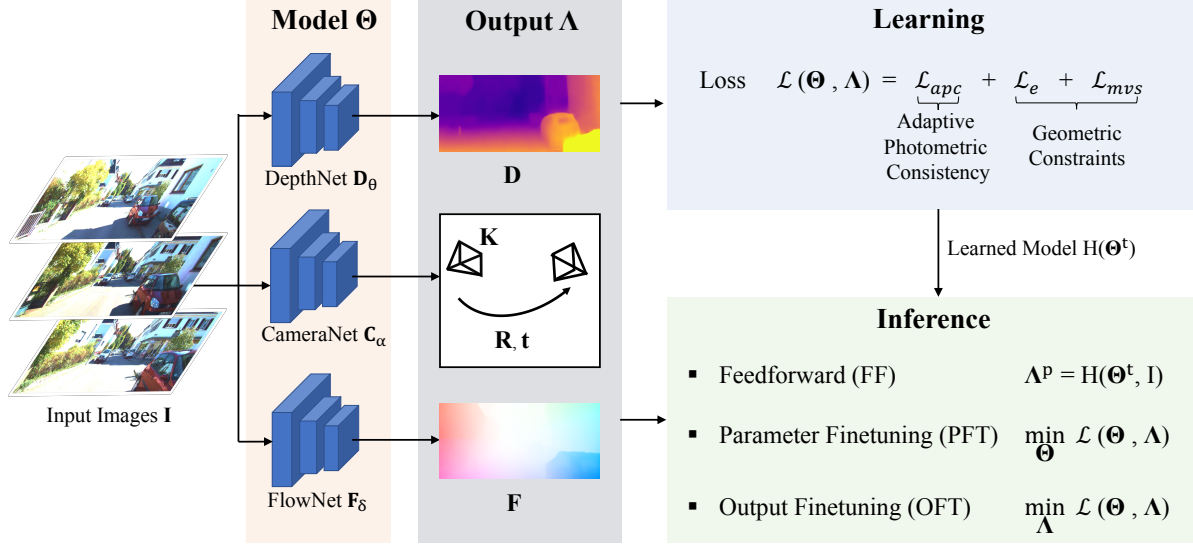


Figure 1. **Overview of the proposed GLNet framework.** The model can take consecutive image frames as input, solves various tasks like depth, camera and flow estimation, and couples them via loss functions that capture the adaptive photometric and geometric constraints among outputs. An important feature of the proposed architecture is its training-testing symmetry as we learn a model in the training stage and during testing we further refine the parameters and the outputs based on the same optimization objective.

matrix writes as

$$\mathbf{K}_\alpha = \begin{bmatrix} f_\alpha^x & 0 & w/2 \\ 0 & f_\alpha^y & h/2 \\ 0 & 0 & 1 \end{bmatrix} \quad (2)$$

Given a pixel \mathbf{p} in the source image I^s , the corresponding 3D scene position in the source camera coordinate system in homogeneous coordinates, can be back-projected as

$$\mathbf{x} = \begin{bmatrix} \mathbf{D}_\theta(\mathbf{p})\mathbf{K}_\alpha^{-1}\mathbf{p} \\ 1 \end{bmatrix} \quad (3)$$

Assuming we displace \mathbf{x} rigidly, the corresponding coordinates (projection) \mathbf{p}' in the target image I^t , are

$$\mathbf{p}' = [\mathbf{K}_\alpha | 0] \mathbf{M}_\alpha \begin{bmatrix} \mathbf{D}_\theta(\mathbf{p})\mathbf{K}_\alpha^{-1}\mathbf{p} \\ 1 \end{bmatrix} \quad (4)$$

In this case, the displacement field $\mathbf{p}' - \mathbf{p}$ represents the 2D projection of the 3D *scene flow*, i.e. the real motion induced by the true underlying 3D rigid displacement.

For pixels that cannot be explained by a rigid transformation, another key quantity is the measured, apparent motion or *optical flow* \mathbf{F}_δ that provides a dense correspondence field between the source and target images

$$\mathbf{p}' = \mathbf{p} + \mathbf{F}_\delta(\mathbf{p}) \quad (5)$$

For simplicity, and in a slight abuse of notation, we also use \mathbf{p} as the 2D (non-homogeneous) image coordinates in the above equation.

3.2. Optimization Objectives

In this section we describe the loss we use for the self-supervised learning of depth, flow, and camera matrix. These tasks are interconnected through photometric and geometric constraints.

Adaptive Photometric Loss The view synthesis loss is widely used in self-supervised learning [48]. The loss is computed as the photometric difference between the synthesized and the actual image, where synthesis is obtained by a 3D reconstruction in the first frame followed by rigid displacement and perspective projection in the second frame. However, this displacement would only be valid for scene structures consistent with the ego-motion, or moving according to a global rigid displacement. For secondary or non-rigidly moving objects, an adaptive approach is necessary and we pursue it here.

Given source and target images I^s and I^t , their pixels belong either to regions explained by ego-motion (or global scene motion), or to secondary dynamic objects. For scene structures with motion not explained by the global rigid motion, one can rely on the more flexible optical flow. The main intuition of our adaptive photometric loss is to channel parameter updates towards only those networks that best explain the displacement, be it produced by either ego-motion or secondary displacements. Thus the term can be represented as the minimum photometric error between the two

displacements (*i.e.* optical flow and rigid motion), as follows

$$\mathcal{L}_{apc} = \min \left\{ S(I^s(\mathbf{p}), I^t(\mathbf{p} + \mathbf{F}_\delta(\mathbf{p}))), \right. \\ \left. S \left(I^s(\mathbf{p}), I^t \left([\mathbf{K}_\alpha | 0] \mathbf{M}_\alpha \begin{bmatrix} \mathbf{D}_\theta(\mathbf{p}) \mathbf{K}_\alpha^{-1} \mathbf{p} \\ 1 \end{bmatrix} \right) \right) \right\} \quad (6)$$

where S is a similarity function between two pixels. As common practice [45, 49], we use a weighted sum of structural similarities (*SSIM*) [41] and L1 components, with trade-off parameter $r = 0.85$, as follows

$$S(a, b) = r \frac{1 - SSIM(a, b)}{2} + (1 - r) \|a - b\|_1 \quad (7)$$

Multi-view 3D Structure Consistency Most previous learning-based structure estimation methods predict depth from a single view, which can be problematic as monocular estimation is inherently ill-posed and scale-ambiguous. To enforce structural consistency, we design a loss component to preserve 3D structure across multiple views.

Given a pixel \mathbf{p} in the source image, and its corresponding pixel in the target image \mathbf{p}' given by (4), their predicted 3D coordinates can be obtained by back-projection, *c.f.* (3). To obtain consistent structure, we penalize deviations between estimates of the same 3D point, once transformed to the common coordinate system of the target camera

$$\mathcal{L}_{mvs} = \|\mathbf{x}' - \mathbf{x}\|_1 = \\ = \left\| \begin{bmatrix} \mathbf{D}_\theta(\mathbf{p}') \mathbf{K}_\alpha^{-1} \mathbf{p}' \\ 1 \end{bmatrix} - \mathbf{M}_\alpha \begin{bmatrix} \mathbf{D}_\theta(\mathbf{p}) \mathbf{K}_\alpha^{-1} \mathbf{p} \\ 1 \end{bmatrix} \right\|_1 \quad (8)$$

The loss represents the 3D discrepancy of predictions from two views, and the gradients are used to update *CameraNet* $\{\mathbf{K}_\alpha, \mathbf{R}_\alpha, \mathbf{t}_\alpha\}$ and *DepthNet* \mathbf{D}_θ . Notice that such a loss can immediately generalize to multiple (more than two) views.

Epipolar Constraint Loss for Optical Flow The epipolar constraint is widely used in classical geometric methods, in order to compute a closed-form solution to initialize non-linear bundle adjustment procedures. Notably absent from existing deep learning-based structure and motion prediction systems, the epipolar constraint is an algebraic relationship that couples 3D scene projections, *e.g.* \mathbf{p} and \mathbf{p}' in two views, via a fundamental or essential matrix, that embeds the geometry of the camera displacement \mathbf{M} and its intrinsic parameters \mathbf{K} . An alternative view of the epipolar constraint, that we leverage in our model, is as a verification equation for putative correspondences, as provided, *e.g.* by optical flow, *c.f.* (5).

Optical flow has been traditionally formulated as an optimization of a matching and smoothness cost, or more recently as per-pixel regression problem within deep-learning

formulations [5, 15]. However, results computed that way may be inconsistent with any epipolar geometry. To endow the learning process with geometric awareness, we incorporate the epipolar constraint as a penalty over dense correspondences computed by optical flow. The resulting epipolar constraint loss writes

$$\mathcal{L}_e = \mathbf{p}^\top \mathbf{K}_\alpha^{-\top} \mathbf{R}_\alpha [\mathbf{t}_\alpha]_\times \mathbf{K}_\alpha^{-1} (\mathbf{p} + \mathbf{F}_\delta(\mathbf{p})) \quad (9)$$

where $[\mathbf{t}]_\times$ is the skew-symmetric matrix corresponding to the translation vector \mathbf{t} . The loss enforces a global epipolar constraint over the dense correspondences from optical flow, the gradients are used to update *CameraNet* $\{\mathbf{K}_\alpha, \mathbf{R}_\alpha, \mathbf{t}_\alpha\}$ and *FlowNet* \mathbf{F}_δ .

Regularization We also rely on standard regularization terms \mathcal{L}_r for our learning framework. Specifically, we use separate spatial smoothness terms over depth \mathbf{D}_θ , and optical flow \mathbf{F}_δ respectively, as well as forward-backward flow consistency constraints.

Total Loss Our total loss is a weighted sum over losses previously introduced, each densely summing over image pixels, with weighting dropped for simplicity

$$\mathcal{L}(\mathbf{\Lambda}, \mathbf{\Theta}) = \mathcal{L}_{apc} + \mathcal{L}_{mvs} + \mathcal{L}_e + \mathcal{L}_r \quad (10)$$

The model is trained jointly in an end-to-end manner.

3.3. Online Optimization

During inference, most existing approaches produce results by running trained models feed-forward. This can be problematic as the structural constraints between multiple outputs, or between inputs and outputs, *e.g.* image intensity, flow, camera motion and depth, are no longer preserved, assuming this happened in training (which, as argued in this paper, has not been entirely the case so far).

Our solution is to operate with – and optimize over – similar losses during both learning and inference, *c.f.* (10). This is possible as our objective is self-supervised, hence it eliminates the asymmetry between training and testing. Therefore an on-line refinement process, either for model parameters, or for model outputs, is possible, and can leverage task dependencies for optimal performance and model adaption to new environments.

Formally, we optimize our model on the training set in order to obtain initial estimates $\mathbf{\Theta}^t$. Giving a test image pair from a monocular video, initial predictions are computed feed-forward in the standard way, as $\mathbf{\Lambda}^p = \{\mathbf{D}^p, \mathbf{F}^p, \mathbf{R}^p, \mathbf{t}^p, \mathbf{K}^p\}$. The (self-supervised) loss in (10) can be computed, as no ground-truth label is needed. To prevent overfitting to the optimization objective, based on a single image pair, we further enforce a regularizer on the output space $\|\mathbf{\Lambda} - \mathbf{\Lambda}^p\|$ in order to penalize large deviation from

the the original prediction of the learned model. The full optimization objective writes as

$$\{\Lambda^*, \Theta^*\} = \arg \min_{\Theta, \Lambda} \mathcal{L}(\Theta, \Lambda) + \|\Lambda - \Lambda^p\| + \|\Theta - \Theta^t\| \quad (11)$$

To update the output, we design two strategies, which can be used together or independently. In **Parameter Fine-tuning (PFT)** we update the parameters of the predictor Θ based on the loss. In **Output Finetuning (OFT)** we optimize the output directly without recomputing the network but with the trained prediction as prior. This is implemented by considering the outputs Λ as free variables, and using the gradient of the loss to refine them. Outputs are initialized with predictions of the trained neural network, but besides initialization, the computational graph associated to the deep model is no longer used. This approach offers the benefit of increased speed, as we only need to run the forward pass through the network once. Moreover, the number of output optimization variables is typically much lower than the number of network parameters, at least for small bundle problems where only several images are jointly optimized.

3.4. Network Architecture

The focus of this work is on different loss functions and fine-tuning options, hence our network design mostly aligns with existing self-supervised learning components for geometric processing. Here we briefly cover the architectures used in this work.

DepthNet maps an input image to a per-pixel depth map. It is based on a fully convolutional encoder-decoder structure. The encoder is based on ResNet18 [14]. The decoder relies on DispNet [28], and consists of several deconvolutional layers. Skip connections are used to provide spatial context, and depth is predicted at multiple scales.

CameraNet takes two adjacent image frames as input, and regresses the 6DOF camera pose, represented as a translation vector and a relative rotation matrix parameterized in terms of three Euler angles. When learning from uncalibrated video, the network also predicts camera intrinsics. As architecture, we use the model of [48] which is a small network with 8 convolutional layers. A global pooling on the last layer is used to acquire the final prediction.

FlowNet predicts the optical flow \mathbf{F} between two adjacent image frames. We use the same architecture described in [45], which is an encoder-decoder with a ResNet backbone.

Note that our framework is agnostic to the particular choice of each component network, and other options are

possible. Our framework would benefit from higher performing networks for individual tasks, or, in principle, from parameter sharing across tasks.

4. Experiments

In this section, we illustrate **GLNet** through extensive experiments on depth, optical flow, and camera pose estimation. We first introduce the datasets and the parameter settings used in our experiments.

Dataset Our experiments are conducted on KITTI [10, 11] and Cityscapes [4]. KITTI is a widely used dataset for benchmarking geometric understanding tasks such as depth estimation, odometry, and optical flow. Images are captured using cameras mounted on cars. We evaluate using the ground-truth labels provided with the official KITTI dataset. We additionally train the framework on Cityscapes [4], and study how well the proposed models transfer across datasets. Similar with KITTI, Cityscapes mainly contains data collected by cars driving in European cities.

Parameter Settings Here we briefly introduce the parameters used in our experiment, we will release the implementation of the proposed work.

The images are resized to 128×416 resolution. Each training sample is a snippet consisting of three consecutive frames.

The loss weight of the adaptive photometric terms is validated to $\lambda_{apc} = 1$, whereas the other loss components are set to 0.1. In training, the network is optimized using Adam [22]. Hyper-parameters are set to $\beta_1 = 0.9$ and $\beta_2 = 0.999$. The initial learning rate is set to 2×10^{-4} and we use a batch of size 4. Additionally, random resizing, cropping, flipping, and color jittering is used during training, as in the common practice of data augmentation. The backbone network is initialized with weights trained on ImageNet, and we optimize the network for maximum 30 epochs although convergence usually occurs earlier.

For online optimization, we initialize the models with weights learned in the training stage. We use a batch size of 1. The batch consists of the test image and its two adjacent frames. Online training is performed for 50 iterations on one test sample with the same hyper-parameter introduced before. No data augmentation is used in the inference phase.

4.1. Depth Estimation

We begin with the evaluation of depth estimation. As common in protocols previously used [48], we report results of depth estimation using the Eigen [7] split of the raw KITTI dataset [10], which consists of 697 test images. Frames that are similar to the test scenes are removed from the training set. We cap depth value larger than 80 meters.

We compare the performance of the proposed framework with two baselines: *baseline* refers to the same net-

	Method	Calib.	Abs Rel ↓	Sq Rel ↓	RMSE ↓	RMSE log ↓	$\delta < 1.25$ ↑	$\delta < 1.25^2$ ↑	$\delta < 1.25^3$ ↑
Trained on KITTI	Zhou <i>et al.</i> * [48]	✓	0.183	1.595	6.709	0.270	0.734	0.902	0.959
	Mahjourian <i>et al.</i> [27]	✓	0.163	1.240	6.220	0.250	0.762	0.916	0.968
	GeoNet [45]	✓	0.155	1.296	5.857	0.233	0.793	0.931	0.973
	Wang <i>et al.</i> [40]	✓	0.151	1.257	5.583	0.228	0.810	0.936	0.974
	LEGO [44]	✓	0.162	1.352	6.276	0.252	-	-	-
	DF-Net [49]	✓	0.150	1.124	5.507	0.223	0.806	0.933	0.973
	Casser <i>et al.</i> [2]	✓	0.109	0.825	4.750	0.187	0.874	0.957	0.982
	<i>Baseline</i>	✓	0.156	1.450	5.913	0.228	0.861	0.931	0.955
	<i>Baseline+ft</i>	✓	0.137	1.077	5.530	0.220	0.826	0.942	0.975
	GLNet	×	0.100	0.811	4.806	0.189	0.875	0.958	0.982
GLNet	✓	0.099	0.796	4.743	0.186	0.884	0.955	0.979	
Trained on CS	GeoNet [45]	✓	0.210	1.723	6.595	0.281	0.681	0.891	0.960
	Casser <i>et al.</i> [2]	✓	0.153	1.109	5.557	0.227	0.796	0.934	0.975
	<i>Baseline</i>	✓	0.206	1.611	6.609	0.281	0.682	0.895	0.959
	<i>Baseline+ft</i>	✓	0.184	1.370	6.278	0.262	0.726	0.909	0.964
	GLNet	×	0.144	1.492	5.473	0.219	0.831	0.932	0.967
	GLNet	✓	0.129	1.044	5.361	0.212	0.843	0.938	0.976

Table 1. Results of depth estimation on the KITTI Eigen Split. We report models trained on KITTI and Cityscapes. The best result in each setting is marked in bold. *The result of Zhou *et al.* [48] is based on their updated Github version.

work architecture but trained only using the standard photometric consistency loss and the regularization terms; *baseline+ft* further finetunes *photometric* at inference time, using ground-truth camera intrinsics. We also compare the results to recent state-of-the-art works in the same setting [2, 27, 40, 44, 45, 48, 49].

Main Results As shown in table 1, our method achieves significant gains over the baseline, as well as the other competing methods, when using ground-truth camera intrinsics (as typical). Qualitative results are shown in fig. 2, where we observe a clear improvement in the visual quality of the depth map. We also notice that *baseline+ft* leads to improvements supporting the observation that online finetuning is effective for depth estimation. This also explains the large gap between Casser *et al.* [2] and other methods, as it is the only approach relying on online finetuning.

In the uncalibrated scenario, where no ground-truth camera intrinsics are given, we use our *CameraNet* network for prediction. The resulting performance matches the calibrated setting. This is a sanity check but not entirely surprising as the camera in the test set has a similar setup with the ones used in training.

The framework is also tested in a transfer learning setting. We train the models self-supervised on Cityscapes, then apply them on KITTI. Again, we observe performance gains when using the proposed components, and overall better results compared to competing methods. This shows the generalization ability of the proposed framework to new environments. It also demonstrates that geometric constraints are powerful in closing domain gaps, as such mathemat-

ical relations are always valid. Interestingly, our method still displays competitive performance when no ground-truth camera calibration is given, even though the camera intrinsics of Cityscapes are different from those of KITTI.

Ablation Study on Loss To analyze the individual impact of each loss component, we provide an ablation study over different combinations of losses. As shown in table 2, our adaptive photometric loss achieves a healthy improvement over the ordinary photometric loss. More importantly, we notice that the proposed loss is especially helpful in dynamic regions, as demonstrated in fig. 3. This is because the proposed loss does not penalize non-rigid regions, where ordinary photometric models do not hold, resulting in artifacts of missing dynamic objects. The performance is further improved by using the geometric loss, especially when coupled with online parameter refinement. Out of the three losses proposed, the multi-view structure consistency seems most effective for depth estimation, which is understandable as it is directly linked to 3D and integrates information over multiple views.

Online Refinement We also conduct an ablation study over refinement strategies. We use the normal parameter finetuning without regularizer as baseline, as used in [2]. We compare the baseline to the two proposed refinement strategies, *i.e.* OFT and PFT. As shown in fig. 4, using standard finetuning we achieve some performance gain, however the downside is rapid overfitting to the test sample. The regularizer can effectively prevent the model from overfit-

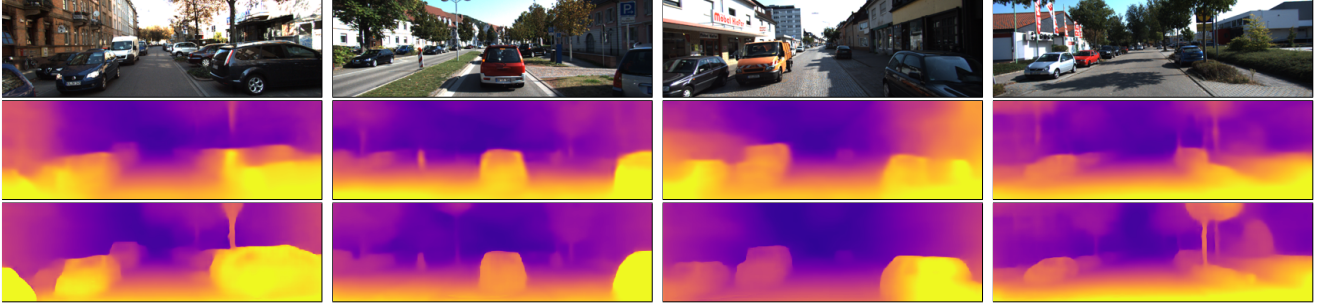


Figure 2. **Qualitative results of depth estimation.** *Top Row:* Input images, *Middle Row:* Baseline results, *Bottom Row:* **GLNet** results. The proposed framework offers sharper predictions.

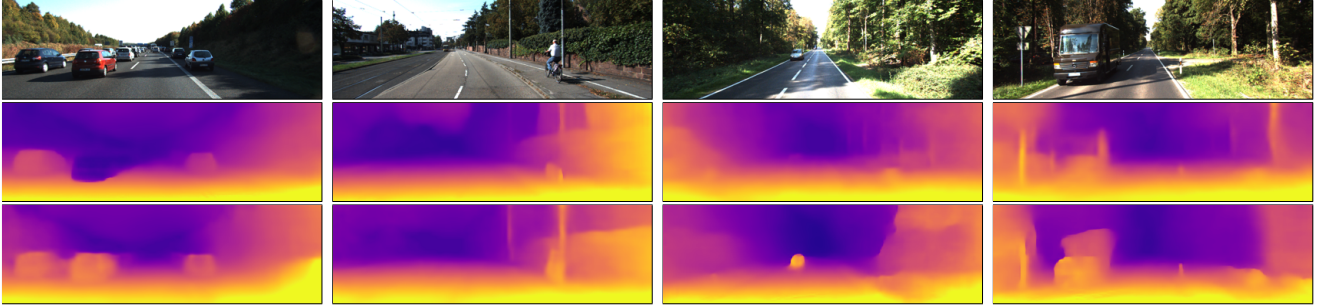


Figure 3. **Illustration of the effect of using the proposed adaptive loss.** *Top Row:* Input images, *Middle Row:* without adaptive loss, *Bottom Row:* with adaptive loss. The results based on the proposed adaptive loss are more precise for the dynamic objects.

\mathcal{L}_{apc}	\mathcal{L}_{mvs}	\mathcal{L}_e	refinement	Abs Rel
				0.156
✓				0.144
✓	✓			0.138
✓	✓	✓		0.135
			✓	0.137
✓			✓	0.130
✓	✓		✓	0.103
✓	✓	✓	✓	0.099

Table 2. **Ablation study on losses.** The results are reported using the Eigen split, on which we evaluate ablated version of the proposed method. Notice the improvements offered by the various components.

ting, for both PFT and OFT. The improvement from OFT is relatively minor compared to other approaches. However, it is much faster compared to the other options as OFT only updates output variables, whose dimensionality is around number of pixels $\sim 10k$. PFT needs to update the parameter of the neural network, whose size is around $\sim 1M$. At runtime, OFT takes about 2 seconds for 50 iterations, whereas OPT typically runs for around 40 seconds for the same number of iterations. Combining PFT and OFT brings some improvement over PFT alone, and achieves the best overall performance.

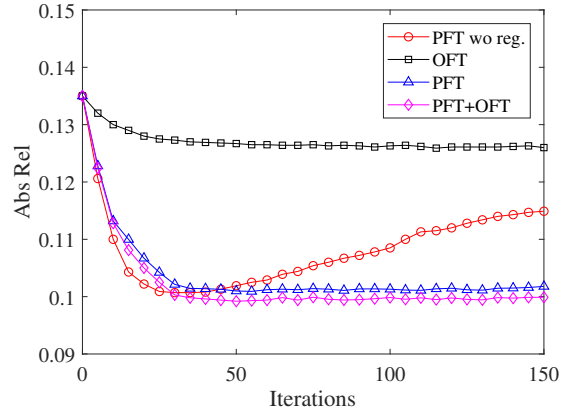


Figure 4. **Study of refinement strategies.** We report the Abs Rel evaluation metric as a function of iteration. Our method achieves the best result and does not overfit to the test sample as refinement proceeds.

Results on Videos in the Wild To further verify the generalization ability of the proposed method, we test **GLNet** on a set of videos collected from Youtube, where the camera intrinsic parameters are unknown. We present some qualitative results of **GLNet** in Figure 5. As can be seen, the proposed method is able to estimate depth from uncalibrated video frames across a variety of objects, structures and scenes. This again suggests that our method can generalize to uncalibrated videos.

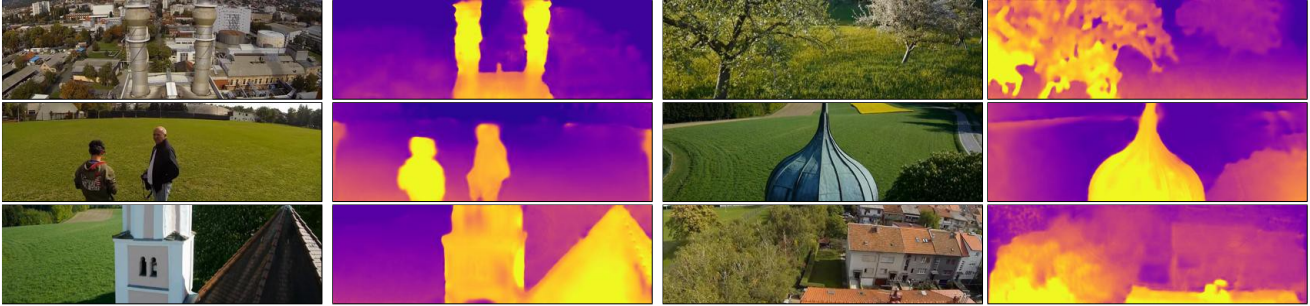


Figure 5. **Qualitative results on Youtube videos, where the camera intrinsics is unknown.** *Left:* Input images, *Right:* Depth estimation results of **GLNet**. The proposed method can robustly estimate depth from uncalibrated videos.

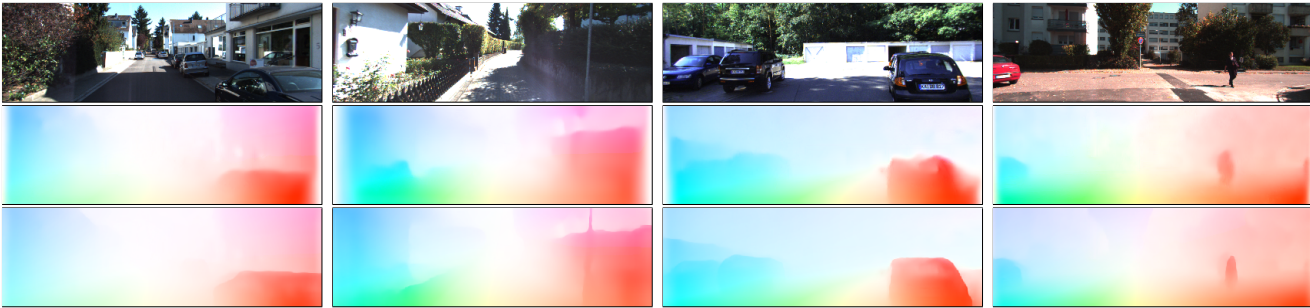


Figure 6. **Qualitative results of flow estimation.** *Top Row:* Input images, *Middle Row:* without geometric constraints, *Bottom Row:* with geometric constraints. The geometric constraints significantly improve the quality of the predicted rigid component flow.

4.2. Optical Flow

To evaluate optical flow, we use the KITTI 2015 stereo/flow training set [30] which has 200 training images. Similarly with previous work [45, 49], we use the training set for evaluation, as the proposed framework is self-supervised.

We report the performance using the average end-point error (EPE) over non-occluded regions (Noc) and overall regions (All). We also use the ordinary photometric consistency with regularizers as a baseline.

As shown in table 3, the proposed adaptive loss and multi-view structure consistency loss don't show much advantage over the baseline, possibly due to their indirect influence on the flow prediction. However, the epipolar constraint loss can achieve considerable performance gain over the baseline. Results can be further improved by online parameter refinement. Notably, the result is even better than the recently proposed DF-Net [49], which is based on a better flow architecture [29] than ours. Our *FlowNet* architecture is identical with the one used in [45], however our results are noticeably better, which demonstrates the effectiveness of our geometric learning framework. Nevertheless, our framework is agnostic to the specific choice of networks, thus more advanced architectures such as PWC-Net [36] can be seamlessly integrated for larger potential gains. Qualitative results are provided in fig. 6, where we can observe that geometric constraints substantially im-

Method	Noc	All
FlowNetS [5]	8.12	14.19
FlowNet2 [15]	4.93	10.06
GeoNet [45]	8.05	10.81
DF-Net [49]	-	8.98
<i>Baseline</i>	6.80	12.28
\mathcal{L}_{apc}	6.78	12.26
$\mathcal{L}_{apc} + \mathcal{L}_{mvs}$	6.77	12.20
$\mathcal{L}_{apc} + \mathcal{L}_{mvs} + \mathcal{L}_e$	5.40	8.95
GLNet	4.86	8.35
GLNet (uncalibrated)	4.90	8.41

Table 3. **Evaluation of optical flow.** We report average end-point error (EPE) on the KITTI 2015 flow training set over non-occluded regions (Noc) and overall regions (All). The first two methods are supervised, and other methods are trained on KITTI unsupervisedly. The best result is marked in bold.

prove the flow quality in the rigid regions. In an uncalibrated setting, the performance is very close to the calibrated one. This is understandable, as the optical flow prediction does not rely on precise intrinsics but can benefit from geometric epipolar corrections which are however calibration-sensitive.

4.3. Pose Estimation Results

We also evaluate the performance of our **GLNet** on the official KITTI visual odometry benchmark. As a standard

Method	Seq.09	Seq.10
ORB-SLAM (full)	0.014 ± 0.008	0.012 ± 0.011
ORB-SLAM (short)	0.064 ± 0.141	0.064 ± 0.130
Zhou <i>et al.</i> [48]	0.016 ± 0.009	0.013 ± 0.009
Mahjourian <i>et al.</i> [27]	0.013 ± 0.010	0.012 ± 0.011
GeoNet [45]	0.012 ± 0.007	0.012 ± 0.009
DF-Net [49]	0.017 ± 0.007	0.015 ± 0.009
Casser <i>et al.</i> [2]	0.011 ± 0.006	0.011 ± 0.010
baseline	0.013 ± 0.007	0.012 ± 0.010
GLNet	0.011 ± 0.006	0.011 ± 0.009

Table 4. **Evaluation on camera pose estimation.** Absolute trajectory error (ATE) on KITTI odometry dataset is reported as the evaluation metrics. Best result is shown in bold.

setting, we use the 00-08 sequences for training, and the 09-10 sequences for testing. Again we use photometric loss as the baseline. The pose estimation results are summarized in table 4, showing improvement over existing methods, as well as our baseline.

5. Conclusions

We have presented **GLNet**, a geometry-inspired learning framework to jointly learn depth, flow, camera pose and intrinsics. The model is self-supervised and combines novel photometric and geometric loss functions, some based on fundamental relations like the epipolar constraint, leveraged in a deep learning framework. We also introduce new parameter and output finetuning methods that break some of the existing asymmetries between training and testing. We have shown the effectiveness of the model for depth, flow and pose estimation, where we report improvements over previous methods. Moreover, we demonstrate that our framework can learn the tasks effectively from uncalibrated video, which is flexible and enables consistent performance across different training and testing domains. This supports the conclusion that geometric constraints represent a valuable regularizer in a transfer learning setting.

References

[1] H. Bay, T. Tuytelaars, and L. Van Gool. SURF: Speeded up robust features. In *ECCV*, 2006. 1

[2] V. Casser, S. Pirk, R. Mahjourian, and A. Angelova. Depth prediction without the sensors: Leveraging structure for unsupervised learning from monocular videos. *arXiv:1811.06152*, 2018. 2, 6, 9

[3] O. Chum, J. Matas, and J. Kittler. Locally optimized ransac. In *Joint Pattern Recognition Symposium*, pages 236–243. Springer, 2003. 2

[4] M. Cordts, M. Omran, S. Ramos, T. Rehfeld, M. Enzweiler, R. Benenson, U. Franke, S. Roth, and B. Schiele. The cityscapes dataset for semantic urban scene understanding. In *CVPR*, 2016. 5

[5] A. Dosovitskiy, P. Fischer, E. Ilg, P. Hausser, C. Hazirbas, V. Golkov, P. Van Der Smagt, D. Cremers, and T. Brox.

FlowNet: Learning optical flow with convolutional networks. In *ICCV*, 2015. 2, 4, 8

[6] D. Eigen and R. Fergus. Predicting depth, surface normals and semantic labels with a common multi-scale convolutional architecture. In *ICCV*, 2015. 2

[7] D. Eigen, C. Puhrsch, and R. Fergus. Depth map prediction from a single image using a multi-scale deep network. In *NIPS*, 2014. 2, 5

[8] Y. Furukawa, B. Curless, S. M. Seitz, and R. Szeliski. Towards internet-scale multi-view stereo. In *CVPR*, 2010. 2

[9] R. Garg, V. K. BG, G. Carneiro, and I. Reid. Unsupervised cnn for single view depth estimation: Geometry to the rescue. In *ECCV*, 2016. 2

[10] A. Geiger, P. Lenz, C. Stiller, and R. Urtasun. Vision meets robotics: The kitti dataset. *The International Journal of Robotics Research*, 32(11):1231–1237, 2013. 1, 2, 5

[11] A. Geiger, P. Lenz, and R. Urtasun. Are we ready for autonomous driving? the kitti vision benchmark suite. In *CVPR*, 2012. 2, 5

[12] C. Godard, O. Mac Aodha, and G. J. Brostow. Unsupervised monocular depth estimation with left-right consistency. In *CVPR*, 2017. 1, 2

[13] R. Hartley and A. Zisserman. *Multiple view geometry in computer vision*. Cambridge university press, 2003. 1, 2

[14] K. He, X. Zhang, S. Ren, and J. Sun. Deep residual learning for image recognition. In *CVPR*, 2016. 5

[15] E. Ilg, N. Mayer, T. Saikia, M. Keuper, A. Dosovitskiy, and T. Brox. FlowNet 2.0: Evolution of optical flow estimation with deep networks. In *CVPR*, 2017. 2, 4, 8

[16] E. Ilg, T. Saikia, M. Keuper, and T. Brox. Occlusions, motion and depth boundaries with a generic network for disparity, optical flow or scene flow estimation. In *ECCV*, 2018. 2

[17] J. Y. Jason, A. W. Harley, and K. G. Derpanis. Back to basics: Unsupervised learning of optical flow via brightness constancy and motion smoothness. In *ECCV*, 2016. 2

[18] A. Kendall and R. Cipolla. Modelling uncertainty in deep learning for camera relocalization. In *ICRA*, 2016. 2

[19] A. Kendall and R. Cipolla. Geometric loss functions for camera pose regression with deep learning. In *CVPR*, 2017. 2

[20] A. Kendall, M. Grimes, and R. Cipolla. PoseNet: A convolutional network for real-time 6-dof camera relocalization. In *ICCV*, 2015. 2

[21] A. Kendall, H. Martirosyan, S. Dasgupta, P. Henry, R. Kennedy, A. Bachrach, and A. Bry. End-to-end learning of geometry and context for deep stereo regression. In *ICCV*, 2017. 2

[22] D. P. Kingma and J. Ba. Adam: A method for stochastic optimization. *arXiv:1412.6980*, 2014. 5

[23] M. Klodt and A. Vedaldi. Supervising the new with the old: learning sfm from sfm. In *ECCV*, 2018. 2

[24] I. Laina, C. Rupprecht, V. Belagiannis, F. Tombari, and N. Navab. Deeper depth prediction with fully convolutional residual networks. In *3DV*, 2016. 2

[25] B. Li, C. Shen, Y. Dai, A. Van Den Hengel, and M. He. Depth and surface normal estimation from monocular images using regression on deep features and hierarchical crfs. In *CVPR*, 2015. 2

- [26] D. G. Lowe et al. Object recognition from local scale-invariant features. In *ICCV*, 1999. 1
- [27] R. Mahjourian, M. Wicke, and A. Angelova. Unsupervised learning of depth and ego-motion from monocular video using 3d geometric constraints. In *CVPR*, 2018. 2, 6, 9
- [28] N. Mayer, E. Ilg, P. Hausser, P. Fischer, D. Cremers, A. Dosovitskiy, and T. Brox. A large dataset to train convolutional networks for disparity, optical flow, and scene flow estimation. In *CVPR*, 2016. 1, 2, 5
- [29] S. Meister, J. Hur, and S. Roth. Unflow: Unsupervised learning of optical flow with a bidirectional census loss. In *AAAI*, 2018. 2, 8
- [30] M. Menze and A. Geiger. Object scene flow for autonomous vehicles. In *CVPR*, 2015. 2, 8
- [31] R. A. Newcombe, S. J. Lovegrove, and A. J. Davison. Dtm: Dense tracking and mapping in real-time. In *ICCV*, 2011. 2
- [32] A. Ranjan and M. J. Black. Optical flow estimation using a spatial pyramid network. In *CVPR*, 2017. 2
- [33] I. Rocco, R. Arandjelovic, and J. Sivic. Convolutional neural network architecture for geometric matching. In *CVPR*, 2017. 2
- [34] S. Ruder. An overview of multi-task learning in deep neural networks. *arXiv:1706.05098*, 2017. 2
- [35] J. L. Schonberger and J.-M. Frahm. Structure-from-motion revisited. In *CVPR*, 2016. 2
- [36] D. Sun, X. Yang, M.-Y. Liu, and J. Kautz. Pwc-net: Cnns for optical flow using pyramid, warping, and cost volume. In *CVPR*, 2018. 2, 8
- [37] B. Triggs, P. F. McLauchlan, R. I. Hartley, and A. W. Fitzgibbon. Bundle adjustment a modern synthesis. In *International workshop on vision algorithms*, pages 298–372. Springer, 1999. 1, 2
- [38] S. Vedula, S. Baker, P. Rander, R. Collins, and T. Kanade. Three-dimensional scene flow. In *ICCV*, 1999. 2
- [39] S. Vijayanarasimhan, S. Ricco, C. Schmid, R. Sukthankar, and K. Fragkiadaki. Sfm-net: Learning of structure and motion from video. *arXiv:1704.07804*, 2017. 2
- [40] C. Wang, J. Miguel Buenaposada, R. Zhu, and S. Lucey. Learning depth from monocular videos using direct methods. In *CVPR*, 2018. 6
- [41] Z. Wang, A. C. Bovik, H. R. Sheikh, E. P. Simoncelli, et al. Image quality assessment: from error visibility to structural similarity. *IEEE transactions on image processing*, 13(4):600–612, 2004. 4
- [42] C. Wu et al. Visualsfm: A visual structure from motion system. 2011. 2
- [43] J. Wulff and M. J. Black. Temporal interpolation as an unsupervised pretraining task for optical flow estimation. *arXiv:1809.08317*, 2018. 2
- [44] Z. Yang, P. Wang, Y. Wang, W. Xu, and R. Nevatia. Lego: Learning edge with geometry all at once by watching videos. In *CVPR*, 2018. 2, 6
- [45] Z. Yin and J. Shi. Geonet: Unsupervised learning of dense depth, optical flow and camera pose. In *CVPR*, 2018. 2, 4, 5, 6, 8, 9
- [46] A. R. Zamir, A. Sax, , W. B. Shen, L. Guibas, J. Malik, and S. Savarese. Taskonomy: Disentangling task transfer learning. In *CVPR*, 2018. 2
- [47] H. Zhan, R. Garg, C. Saroj Weerasekera, K. Li, H. Agarwal, and I. Reid. Unsupervised learning of monocular depth estimation and visual odometry with deep feature reconstruction. In *CVPR*, 2018. 2
- [48] T. Zhou, M. Brown, N. Snavely, and D. G. Lowe. Unsupervised learning of depth and ego-motion from video. In *CVPR*, 2017. 1, 2, 3, 5, 6, 9
- [49] Y. Zou, Z. Luo, and J.-B. Huang. Df-net: Unsupervised joint learning of depth and flow using cross-task consistency. In *ECCV*, 2018. 2, 4, 6, 8, 9